ISSN 1330-3651 (Print), ISSN 1848-6339 (Online) https://doi.org/10.17559/TV-20230917000943
Original scientific paper

Interval Fatigue Life Prediction of Dissimilar Metal Cruciform Welded Joints under Impact Loading

Liuping WANG, Zhengshun NI, Zhiyuan ZHANG, Ling ZHANG, Yingjian DENG, Jiping WU, Tao XIONG, Ningning LIAO, Chengji MI*

Abstract: In order to characterize the local damage and fatigue strength of 5754 and 5052 aluminum alloy cross-welded joints containing pre-cracks under impact loading, an interval fatigue life prediction approach is presented based on the continuum damage mechanics and the uncertain interval analysis technique. The impact test is carried out on the cruciform welded joints of dissimilar lightweight metals with U-type pre-crack located at the middle edge of specimen. In consideration of uncertain factors caused by the welding process, the interval fatigue damage model under the coupling effect of fatigue and impact load is established. Then, the interval fatigue parameters and interval curve between stress amplitudes and fatigue life are determined. The impact process is simulated by using the finite element dynamic analysis to obtain the stress and plastic strain fields. Based on the suggested model, the predicted results agree well with the experimental data.

Keywords: continuum damage mechanics; fatigue life; impact; interval approach; welded joints

1 INTRODUCTION

In engineering structure, dissimilar light metal plates are widely connected by the welding. However, because of assembly loosening or suffering impact from the external load, the welded joints are subjected to cyclic and impact loading. In fact, there are uncertain factors during the welding process, which produce the challenge for accurately evaluating fatigue life of welded joints, especially under the coupling effect of fatigue and impact loading [1-3].

Based on the continuum mechanics and thermodynamics, researchers have established a theoretical model of damage mechanics and developed a corresponding life prediction method. The purpose of continuous damage mechanics is to study the mechanical properties of damaged materials or components to explore the regularity and mechanisms between the initial damage and fatigue failure of components [4]. This defined damage parameter can reveal the changes and behaviors of materials during the fatigue damage accumulation, and describe the coupling effect between the damage field and stress field [5, 6]. A phase-field approach to study ductile fracture and fatigue failure in a non-traditional thermodynamic framework is proposed, coupling the damage evolution with developing of plastic strain, and the validity of the model is verified by various numerical examples and compared with experimental data [7]. A comprehensive finite element method based on the theory of continuum damage mechanics (CDM) and linear elastic fracture mechanics (LEFM) is presented to predict the total bending fatigue life of gears, including crack initiation and extension, and the results show that the period of crack initiation life depends on the load level [8, 9]. Moreover, the crack initiation life of gears in bending fatigue occupies a dominant position in the total fatigue life [10, 11]. A new numerical analysis method to simulate ship collisions and groundings based on CDM is suggested by adding new internal variables into the constitutive equations, relating to the damage produced by the stress field [12].

The traditional design methods mentioned above focus on deterministic fatigue life estimation based on the certain material properties. However, the artificial welding process is prone to result in uncertain factors [13]. In this paper, based on the interval analysis method and CDM, an interval fatigue life assessment model is presented to analyze the accumulative damage of dissimilar metal cruciform welded joints with U-type pre-crack under impact loading. According to the testing data and the simulated results, the interval fatigue parameters and interval curve between stress amplitudes and fatigue life are determined. Based on the suggested model, the evaluated results are compared with the experimental data.

2 EXPERIMENTAL WORK

2.1 Mechanical Properties

In this paper, 5052 aluminum alloy and 5754 aluminum alloy are considered as the base materials, because of good absorption of impact effect, as well as good formability and corrosion resistance. The chemical compositions and mechanical properties of two parental metals are listed in Tab. 1 and Tab. 2 [14-16], respectively.

The load-bearing aluminum alloy cruciform welded joints are connected by manual MIG. The welding area is in advance polished with sandpaper to remove oxide film and oil and wiped with acetone. The welding current is within 210-220 A, and the welding voltage is 24 V.

Table 1 Chemical compositions of two parental materials (%)

	Mg	Mn	Cr	Si	Cu	Fe	Zn	Al
5052	2.55	0.10	0.20	0.25	0.10	0.33	0.07	Bal.
5754	3.40	0.50	0.01	0.10	0.04	0.30	—	Bal.

Table 2 Mechanical properties of 5052 and 5754 aluminium alloys

	Modulus of elasticity / GPa	Yield strength	Modulus of elasticity / GPa	Poisson's ratio
5052	70.3	193.0	228.0	0.3
5754	61.0	117.0	195.0	0.3

The wire type was ER5356, while the wire diameter is 1 mm. The wire feeding speed is matched to the welding current, and Argon is used as the protective gas. The 5052 aluminum alloy is used as the carrier plate and the 5754 aluminum alloy is considered as the non-carrier plate. The dimension of load-bearing aluminum alloy cruciform welded joint is shown in Fig. 1. The effective area is 40 mm^2, while the thickness of plate is 4 mm.

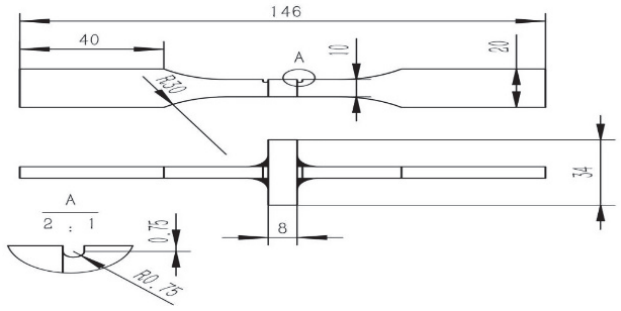

Figure 1 Dimension of load-bearing cross-welded joint

According to the dimension of designed cruciform welded joint, the pre-cracks located at the end of weld seam are machined by the EDM wire cutting. Then, an U-shaped pre-crack with a depth of 1.5 mm, a width of 1.5 mm and a top radius of 0.75 mm is performed in the welded region on both sides of the cross-welded joints, and the specimen is shown in Fig. 2.

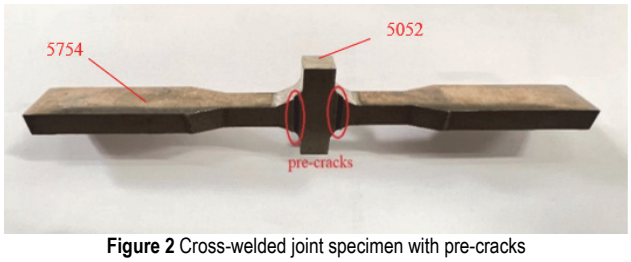

Figure 2 Cross-welded joint specimen with pre-cracks

The monotonic tensile test is conducted on the cruciform welded joint, and the stress-strain curve is shown in Fig. 3. Then, the modulus of elasticity is around 62.3 GPa, the yield and tensile strength is 138.2 MPa, and 189.6 MPa, respectively. The mechanical properties of welded joint are close to the parental material.

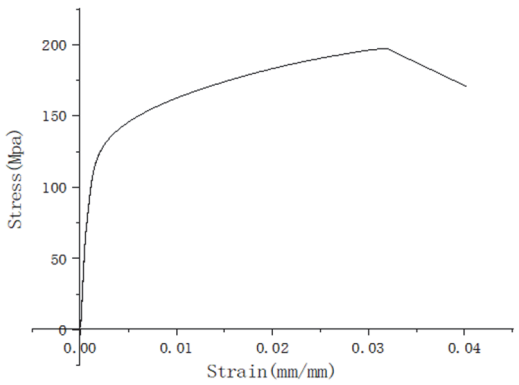

Figure 3 Stress-strain curve of cross-welded joints under monotonic tensile test

2.2 Impact Test

The impact test is aimed to simulate the damage caused by a falling object from a vertical direction to the specimen, while the pre-cracking of the welded joint is backed to the impact surface. In general, the hardness of impacting body is much greater than the load-bearing cross-welded joint of dissimilar metal. Therefore, the rigid ball with a weight of 350 g drops on one side of welded joints in the form of a free fall at a height of 800 mm. The radius of ball is 35 mm, and the material is 304L stainless steel. In order to protect the specimen, the ball falls along the hollow pipeline without contact, and the testing bench is shown in Fig. 4 [17]. The impacted cruciform welded joint is compared with the non-impacted welded joint, as shown in Fig. 5. Then, the deformation caused by the impact process could be determined, as shown in Fig. 6.

Figure 4 Impact test bench

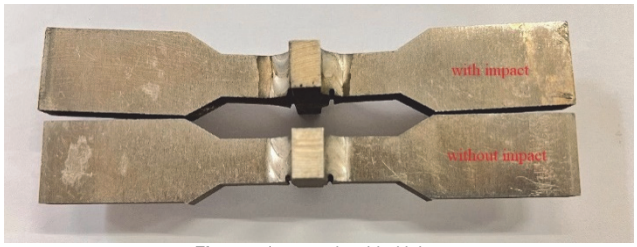

Figure 5 Impacted welded joint

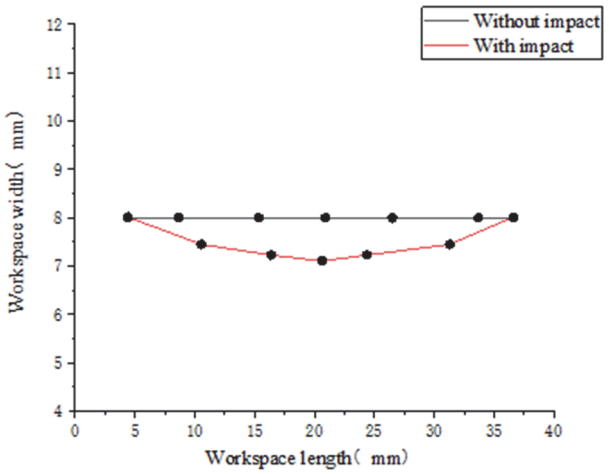

Figure 6 Deformation of impacted cruciform welded joint

2.3 Fatigue Test

According to the Chinese standard [18], the fatigue tests are conducted on the impacted cross-welded joints with U-shaped pre-crack. The stress ratio is 0.1, and the loading frequency is 2 Hz. All tests are performed at room temperature of 25 °C, and are under stress control. If the load change reaches 80%, the test would be ended. Then, the cyclic data is listed in Tab. 3.

Fatigue fracture morphology of specimen 2 is shown in Fig. 7. It is clearly seen that the fatigue cracks start from the notch location, expanding towards the impact contact surface. Apparently, the pre-cracks produce damage in the welded zone. However, the traditional fatigue life prediction method based on the S-N curve does not include the initial damage, and the welding process can result in the uncertain parameters. How to accurately estimate the remaining life of pre-cracked cruciform welded joint under impact and cyclic loading is discussed in the following part.

Table 3 Fatigue life data of impacted welded joints

Specimen No.	Stress amplitude / MPa	Fatigue life/cycles
1	70	282108
2	80	163694
3	90	92483
4	100	68957
5	110	49324
6	120	35126
7	130	26670
8	140	19585
9	150	8985
10	160	4326

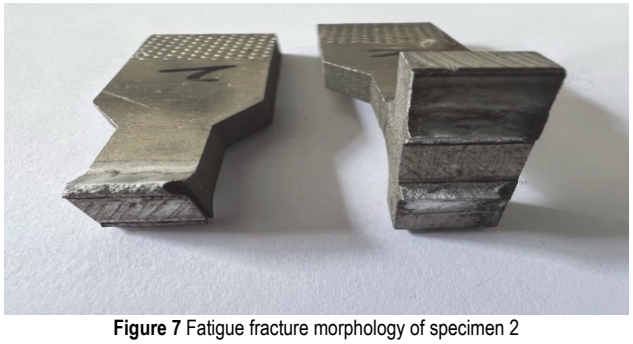

Figure 7 Fatigue fracture morphology of specimen 2

3 INTERVAL FATIGUE LIFE ESTIMATION

3.1 Interval Fatigue Life Prediction Model

Based on the continuum damage mechanics, the damage model could be described as [17]:

$$N_f = \frac{1}{(1-\alpha)(1+\beta)}\left[\frac{M(\sigma_m)}{\sigma_a}\right]^{\beta} \left\{1-\left[1-(1-D_0)^{1+\beta}\right]^{1-\alpha}\right\} \tag{1}$$

where M is the function of mean stress σ_m, σ_a is stress amplitude, D_0 is initial damage, α and β is material parameters, respectively. In this paper, parameter α and β is equal to 0.969 and 1.601 [17].

Then, Eq. (1) could be simplified as:

$$N_f = a\sigma_a^b \tag{2}$$

where a and b is fatigue life coefficient and fatigue life index.

In order to characterize the uncertainties of welding process, the interval analysis method is utilized to renew the fatigue life model. Further, Eq. (2) could be changed as:

$$\log_{10}(\sigma_a) = B\log_{10}(N_f) + \log_{10} A \tag{3}$$

Based on the first-order least squares method, Eq. (3) can be transformed into [19]:

$$y_i = \beta_{1i}x_i + \beta_{2i}, (i = 1,2,3...N) \tag{4}$$

where β_{1i} denotes the slope of the first order function, β_{2i} denotes the constant term of the first order function.

Vectorizing the scalar Eq. (4), it can be expressed as [19]:

$$X\beta = y \tag{5}$$

$$X = \begin{bmatrix} x_1 & 1 \\ x_2 & 1 \\ x_3 & 1 \\ \vdots & \vdots \\ x_N & 1 \end{bmatrix} = \begin{bmatrix} \log_{10}(N_{f1}) & 1 \\ \log_{10}(N_{f2}) & 1 \\ \log_{10}(N_{f3}) & 1 \\ \vdots & \vdots \\ \log_{10}(N_{fn}) & 1 \end{bmatrix}, \quad y = \begin{bmatrix} y_1 \\ y_2 \\ y_3 \\ \vdots \\ y_N \end{bmatrix} = \begin{bmatrix} \log_{10}(\partial_{a_1}) \\ \log_{10}(\partial_{a_2}) \\ \log_{10}(\partial_{a_3}) \\ \vdots \\ \log_{10}(\partial_{a_N}) \end{bmatrix}, \beta = \begin{bmatrix} \beta_1 \\ \beta_2 \end{bmatrix} \tag{6}$$

Then, the vectorized equation can be determined as [19]:

$$X^T X\hat{\beta} = X^T y \tag{7}$$

$$\hat{\beta} = \left(X^T X\right)^{-1} X^T y \tag{8}$$

The regression coefficient can be calculated as follows [19]:

$$\hat{\beta}_1 = \frac{\overline{xy} - \overline{x}\,\overline{y}}{\overline{x^2} - \overline{y^2}} \tag{9}$$

$$\hat{\beta}_2 = \overline{y} - \hat{\beta}_1\overline{x} \tag{10}$$

$$\overline{x} = \sum x/n, \overline{y} = \sum y/n \tag{11}$$

Then, based on the least-squares method, the obtained fatigue test data could be expanded. The fitted parameters β_{1i} and β_{2i} under different omitted sample points can be rearranged, and thus Eq. (3) can be established as [19]:

$$\log_{10}\left(\partial_{a_k}^{i,j}\right) = \hat{\beta}_1^{i,j}\log_{10}\left(N_{f_k}\right) + \hat{\beta}_2^{i,j} \tag{12}$$

where $i \in 1,2,3,...,m; j \in 1,2,3,...,n; k \in 1,2,3,...,N$, m

denotes the number of omitted points, n denotes the number of rearranged combinations after omitted points, and N denotes the total number of sample points.

The smallest $\log_{10}\left(\partial^{i,j}_{a_k\min}\right)$ and the largest $\log_{10}\left(\partial^{i,j}_{a_k\max}\right)$ can be calculated as [19]:

$$\log_{10}\left(\partial^{i}_{a_k\min}\right)=\min\begin{pmatrix}\log_{10}\left(\partial^{i,1}_{a_k}\right),\log_{10}\left(\partial^{i,2}_{a_k}\right),\\ ...,\log_{10}\left(\partial^{i,n}_{a_k}\right)\end{pmatrix} \tag{13}$$

$$\log_{10}\left(\partial^{i}_{a_k\max}\right)=\max\begin{pmatrix}\log_{10}\left(\partial^{i,1}_{a_k}\right),\log_{10}\left(\partial^{i,2}_{a_k}\right),\\ ...,\log_{10}\left(\partial^{i,n}_{a_k}\right)\end{pmatrix} \tag{14}$$

Then, the dependent variable y_i can be expressed as [19]:

$$y_{i\min}=\begin{bmatrix}\log_{10}\left(\partial^{i}_{a1\min}\right)\\ \log_{10}\left(\partial^{i}_{a2\min}\right)\\ \vdots\\ \log_{10}\left(\partial^{i}_{aN\min}\right)\end{bmatrix} \tag{15}$$

$$y_{i\max}=\begin{bmatrix}\log_{10}\left(\partial^{i}_{a1\max}\right)\\ \log_{10}\left(\partial^{i}_{a2\max}\right)\\ \vdots\\ \log_{10}\left(\partial^{i}_{aN\max}\right)\end{bmatrix} \tag{16}$$

Then, based on the obtained data sets, the new coefficients $\hat{\beta}_{i1}$, $\hat{\beta}_{i2}$ can be defined by using the least-squares method to characterize the interval values of the uncertain fatigue parameters [19]:

$$\hat{\beta}_{i1}=\left(X^TX\right)^{-1}X^Ty_{i\min},\hat{\beta}_{i2}=\left(X^TX\right)^{-1}X^Ty_{i\max} \tag{17}$$

Finally, the inveral bounds of two fitting parameters can be described as [19]:

$$\beta_1^l=\min\left(\hat{\beta}_{i1_1},\hat{\beta}_{i2_1}\right),\beta_1^u=\max\left(\hat{\beta}_{i1_1},\hat{\beta}_{i2_1}\right) \tag{18}$$

$$\beta_2^l=\min\left(\hat{\beta}_{i1_2},\hat{\beta}_{i2_2}\right),\beta_1^u=\max\left(\hat{\beta}_{i1_2},\hat{\beta}_{i2_1}\right) \tag{19}$$

$$\beta_{i1}=\left[\beta_1^l,\beta_1^u\right],\beta_{i2}=\left[\beta_2^l,\beta_2^u\right] \tag{20}$$

According to the equations mentioned above and fatigue life data sets, the interval fatigue life curve of cross-welded joints is obtained, as shown in Fig. 8. The nominal stress is the maximum tensile force divided by the effective area. The upper and lower limit of the interval curve includes all experimental data, except only one point stays on the lower boundary line. It could be clearly seen that the interval fatigue life prediction curve can cover all sample points.

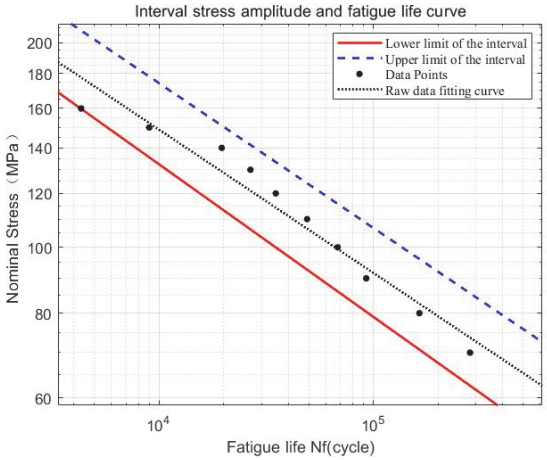

Figure 8 Interval fatigue life curve

3.2 Simulation of Impact Process

In order to study the anti-impact performance of dissimilar metal cruciform welded joints with U-type pre-crack, the dynamic finite element analysis is performed to obtain the stress and strain field. The rigid ball is considered as a discrete rigid body, while the welded joint is taken as an elasto-plastic body. Based on the software ABAQUS, the finite element model of welded joint with pre-cracks is built. The contact surface between rigid ball and welded joint is located in the middle of specimen, and its meshes are refined. Finally, the model has 30214 elements, and 48232 nodes. The eight-node linear hexahedral cell (C3D8R) is used to simulate the solid part, as shown in Fig. 9.

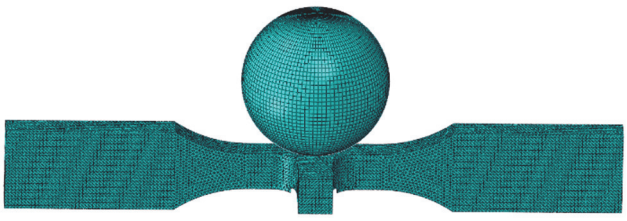

Figure 9 Finite element model of impact simulation

The material properties of welded joint are from Fig. 3. The rigid body starts to move as the free-fall at the height of 800 mm. Two ends of specimen are fixed. Then, based on the transient dynamics analysis, the stress and strain field of dissimilar metal cruciform welded joints with U-type pre-crack after impacting is obtained, as shown in Fig. 10, Fig. 11, Fig. 12 and Fig. 13, respectively. From the stress field, it could be clearly seen that the maximum stress is 198.6 MPa, and attends at the crack tip. The structural stress level reaches 185 MPa, which exceeds its yield strength and produces the initial damage. Moreover, the maximum equivalent plastic strain is 0.2389 mm/mm, which is located at the contact surface between rigid body

and welded joint. The irreversible plastic strain would contribute to the cumulative damage.

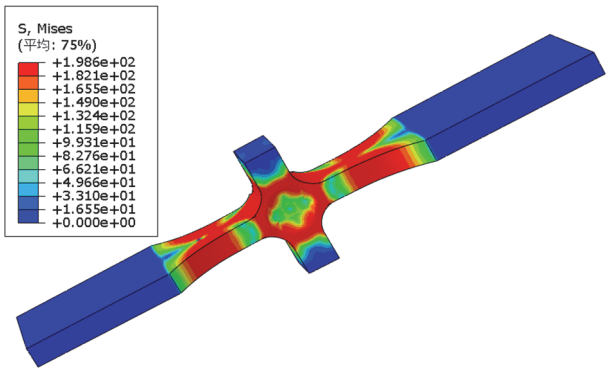

Figure 10 Stress field on impact contact surface

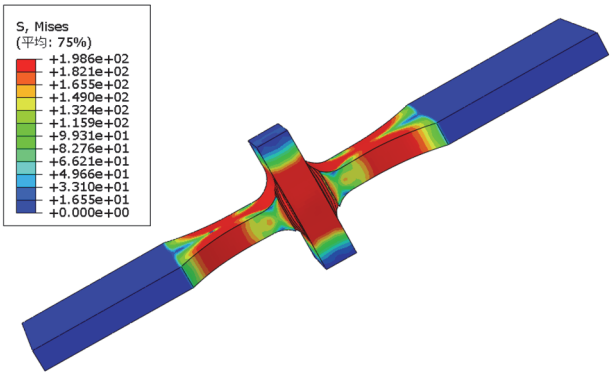

Figure 11 Stress field on back of impact contact surface

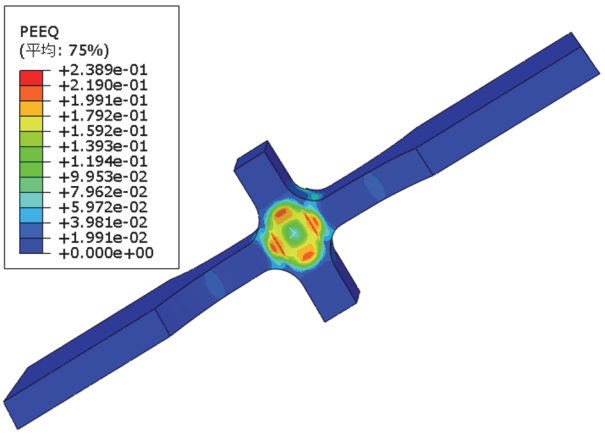

Figure 12 Strain field on impact contact surface

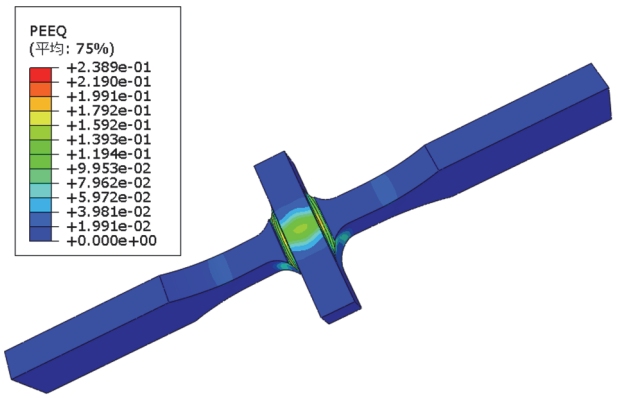

Figure 13 Strain field on back of impact contact surface

3.3 Interval Lifetime Estimation

In order to further verify the accuracy of the interval model mentioned above, the fatigue life estimation of impacted cross-welded joints containing pre-cracks is performed. Based on Eq. (2) and interval fatigue life curve of dissimilar metal cruciform welded joints, the predicted results are shown in Fig. 14. The lower and upper bound values at stress amplitude of 75 MPa, 85 MPa, 95 MPa, 105 MPa, 115 MPa, 125 MPa, 135 MPa, 145 MPa, 155 MPa and 165 MPa are determined. Then, according to the Chinese standard, the cooresponding fatigue tests at the same stress amplitude are conducted, and the experimental data is compared with the estimated results. It could be clearly seen that the fatigue life distribution is comparatively uniform, and most of the actual fatigue life is in the middle of the predicted interval, which verifies the effectiveness of the method proposed in this paper. The overall calculated results based on the interval fatigue life model are in good agreement with the tested data, which also shows that the combination of the fatigue life prediction model based on continuous damage mechanics and the interval analysis method can provide more accurate and fast fatigue life prediction.

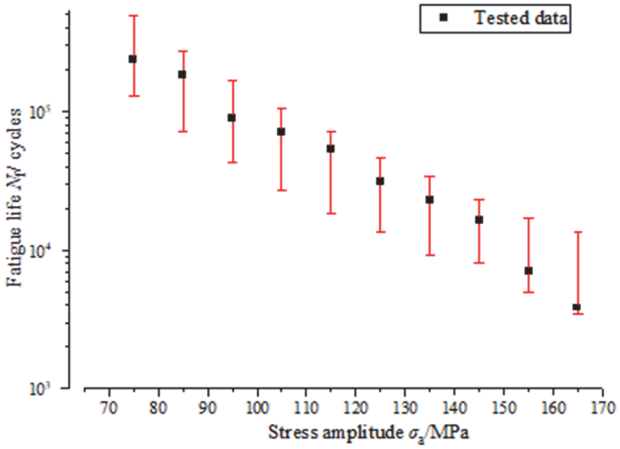

Figure 14 Interval fatigue life predicted results

4 CONCLUSION

In this paper, in order to exactly predict the fatigue life of dissimilar lightweight metal cross-welded joints containing pre-cracks under impact loading, an interval fatigue life prediction approach is presented based on the continuum damage mechanics and the uncertain interval analysis technique. The 5754 aluminum alloy and 5052 aluminum alloy are considered as the parental materials to make the cruciform welded joints with U-type pre-cracks. Then, the mechanical properties of welded joint are determined by the monotonic tensile test, the impact characteristics are obtained by the free-falling ball impact test and the fatigue tests at ten stress amplitudes are performed in accordance with the Chinese standard. The stress and strain field of the load-bearing cruciform welded joints after impacting is determined by the transient dynamic analysis. In consideration of uncertain factors caused by the welding process, the interval analysis method is utilized to construct the interval fatigue life model based on the continuous damage mechanics. The

upper and lower bound values of uncertain parameters in the model are determined. Finally, according to the suggested model, the interval fatigue life of load-bearing cruciform welded joints after impacting at other ten stress amplitudes is conducted, while the predicted results agree well with the experimental data.

Nomenclature

M - The function of mean stress σ_m
σ_a - Stress amplitude
D_0 - Initial damage
α - Material parameters equal to 0.969
β - Material parameters equal to 1.601
a - Fatigue life coefficient
b - Fatigue life index
β_{1i} - Denotes the slope of the first order function
β_{2i} - Denotes the constant term of the first order function
m - Denotes the number of omitted points
n - Denotes the number of rearranged combinations after omitted points
N - Denotes the total number of sample points

Acknowledgements

This work was funded by the Natural Science Foundation of Hunan Province (No.:2021JJ50042 and 2023JJ50186 and 2021JJ40181), the Postgraduate Research Innovation Project of Hunan Province (No.: CX20220850), and the Scientific Research Project of Hunan Provincial Education Department (No.: 21A0362 and 22C0797).

5 REFERENCES

[1] Branco, R., Costa, J. D., Borrego, L. P., Berto, F., Razavi, S. M. J., & Macek, W. (2021). Comparison of different one-parameter damage laws and local stress-strain approaches in multiaxial fatigue life assessment of notched components. *International Journal of Fatigue*, *151*,106405. https://doi.org/10.1016/j.ijfatigue.2021.106405

[2] Savkovic, M., Gasic, M., Petrovic, D., Zdravkovic, N., & Pljakic, R. (2012). Analysis of the drive shaft fracture of the bucket wheel excavator. *Engineering Failure Analysis*, (20), 105-117. https://doi.org/10.1016/j.engfailanal.2011.11.004

[3] Sertić, J., Samardžić, I., Kozak, D., Šimunić, D., Gelo, I., & Bučević-Keran, D. (2015). Influence of fatigue impact loading on radial carrier and rapping device fillet weld strength. *Tehnički vjesnik*, *22*(2), 547-555. https://doi: 10.17559/TV-20141022092231

[4] Ghidini, T. & Donne, C. D. (2009). Fatigue life predictions using fracture mechanics methods. *Engineering Fracture Mechanics*, (76), 134-148. https://doi.org/10.1016/j.engfracmech.2008.07.008

[5] Eufinger, J., Heinrietz, A., Bruder, T., & Hanselka, H. (2012). An engineering approach to fatigue analysis based on elastic-plastic fracture mechanics. *Fatigue & Fracture of Engineering Materials & Structures*, (36), 65-74. https://doi.org/10.1111/j.1460-2695.2012.01680.x

[6] Berto, F., Razavi, S. M. J., & Torgersen, J. (2018). Frontiers of fracture and fatigue: Some recent applications of the local strain energy density. *Fractured Integrity Structural*, (43), 1-32. https://doi.org/10.3221/IGF-ESIS.43.01

[7] Aris, T. & Michael, V. (2023). Phase field modelling of ductile fracture in the frameworks of non-conventional thermodynamics and continuum damage mechanics. *International Journal of Solids and Structures*, 262-263. https://doi.org/10.1016/j.ijsolstr.2022.112049

[8] He, H. F., Liu, H. J., Andrea, M., & Zhu, C. C. (2022). Gear bending fatigue life prediction based on continuum damage mechanics and linear elastic fracture mechanics. *Meccanica*, *58*(1), 119-125. https://doi.org/10.1007/s11012-022-01622-5

[9] Sghayer, A., Grbovic, A., Sedmak, A., Dinulovic, M., Grozdanovic, I., Sedmak, S., & Petrovski, B. (2018). Experimental and Numerical Analysis of Fatigue Crack Growth in Integral Skin-Stringer Panels. *Tehnički vjesnik*, 25(3), 785-791. https://doi.org/10.17559/TV-20170308110329

[10] Voyiadjis, G. Z. & Kattan, P. I. (2019). Fundamental aspects for characterization in continuum damage mechanics. *International Journal of Damage Mechanics*, *0*(0), 1-19. https://doi.org/10.1177/1056789517752524

[11] Drobne, M., Gubeljak, N., & Glodež, S. (2014). Experimental determination of fatigue parameters of high chromium steel under different loading and temperature conditions. *Tehnički vjesnik*, 21(4), 853-860. https://doi.org/0000-0002-3276-8431

[12] Martinez, J. L., Cyrino, J. C. R., & Vaz, M. A. (2017). Continuum damage mechanics applied to numerical analysis of ship collisions. *Marine Structures*, *56*. https://doi.org/10.1016/j.marstruc.2017.08.003

[13] Guerine, A., Hami, A. E, Walha, L., Fakhfakh, T., & Haddar, M. (2017). Dynamic response of wind turbine gear system with uncertain-but-bounded parameters using interval analysis method. *Renewable Energy*, *113*, 679-687. https://doi.org/10.1016/j.renene.2017.06.028

[14] Abdel-Rahman, M., Salah, M., & Ibrahim, A. M. (2017). Comparative techniques to investigate plastically deformed 5754 Al-alloy. *Modern Physics Letters B*, *31*(28),1750255. https://doi.org/10.1142/S0217984917502554

[15] Yogesha, K. K., Amit, J., Raja, A., Jayaganthan, R., & Raviraj, V. (2022). Effect of Different Rolling Techniques on Fatigue Crack Propagation in 5052 Al Alloy. *Metallography, Microstructure, and Analysis*, *12*(1), 62-73. https://doi.org/10.1007/s13632-022-00918-y

[16] Bertrand, D., Bourrier, F., Olmedo, I., Brun, M., & Berger, F., & Limam, A. (2013). Experimental and numerical dynamic analysis of a live tree stem impacted by a Charpy pendulum. *International Journal of Solids and Structures*, *50*(10),1689-1698. https://doi.org/10.1016/j.ijsolstr.2013.01.037

[17] Ni, Z. S., Xiong, T., Lei, J., Wang, L. P., Gao, T., Yu, J. W., & Mi, C. J. (2022). Life prediction method of dissimilar lightweight materials welded joints with pre-crack under coupled impact-fatigue loading. *Materials*, *15*, 5077. https://doi.org/10.3390/ma15145077

[18] Mi, C. J., Li, Y. Q., Zhang, C., Zhang, D., Liu, X. H., Hu, X. L., & Zhang, D. J. (2023). An energy-based anti-fatigue optimization desing method of welded rear axle housing in a mining dump truck. *Mechanika*, 29(4), 317-323. https://doi.org/10.5755/j02.mech.32371

[19] Gu, Z. Q. & Ma, X. K. (2018). A feasible method for the estimation of the interval bounds based on limited strain-life fatigue data. *International Journal of Fatigue*, 116, 172-179. https://doi.org/10.1016/j.ijfatigue.2018.06.024

Contact information

Liuping WANG
Department of Mechanical Engineering,
Hunan University of Technology,
No. 88 West of Taishan Road, Zhuzhou City, China
E-mail: wangliuping_hut@126.com

Zhengshun NI
Department of Mechanical Engineering,
Hunan University of Technology,
No. 88 West of Taishan Road, Zhuzhou City, China
E-mail: nizhengshun@126.com

Zhiyuan ZHANG
Department of Mechanical Engineering,
Hunan University of Technology,
No. 88 West of Taishan Road, Zhuzhou City, China

Ling ZHANG
Key Laboratory of High-performance rolling bearings in Hunan Province,
Hunan University of Technology,
No. 88 West of Taishan Road, Zhuzhou City, China

Yingjian DENG
Department of Mechanical Engineering,
Hunan University of Technology,
No. 88 West of Taishan Road, Zhuzhou City, China

Jiping WU
Key Laboratory of High-performance rolling bearings in Hunan Province,
Hunan University of Technology,
No. 88 West of Taishan Road, Zhuzhou City, China

Tao XIONG
Zhuzhou Guochuang Rail Technology Co., Ltd.,
Zhuzhou City, China 412000

Ningning LIAO
Zhuzhou Guochuang Rail Technology Co., Ltd.,
Zhuzhou City, China 412000

Chengji MI
(Corresponding Author)
Department of Mechanical Engineering,
Hunan University of Technology,
No. 88 West of Taishan Road, Zhuzhou City, China
E-mail: michengji_86@126.com